

LiMn_{1-x}Fe_xPO₄ Nanorods Grown on Graphene Sheets for Ultrahigh-Rate-Performance Lithium Ion Batteries**

Hailiang Wang, Yuan Yang, Yongye Liang, Li-Feng Cui, Hernan Sanchez Casalongue, Yanguang Li, Guosong Hong, Yi Cui,* and Hongjie Dai*

Olivine-type lithium transition-metal phosphates LiMPO₄ (M = Fe, Mn, Co, or Ni) have been intensively investigated as promising cathode materials for rechargeable lithium ion batteries (LIBs) owing to their high capacity, excellent cycle life, thermal stability, environmental benignity, and low cost.^[1–19] However, the inherently low ionic and electrical conductivities of LiMPO₄ seriously limit Li⁺ insertion and extraction and charge transport rates in these materials. In recent years, these obstacles have been overcome for LiFePO₄ by reducing the size of LiFePO₄ particles to the nanoscale and applying conductive surface coatings such as carbon, which leads to commercially viable LiFePO₄ cathode materials.^[5–13]

Compared to LiFePO₄, LiMnPO₄ is an attractive cathode material owing to its higher Li⁺ intercalation potential of 4.1 V versus Li⁺/Li (3.4 V for LiFePO₄), providing about 20% higher energy density than LiFePO₄ for LIBs.^[14–19] Importantly, the 4.1 V intercalation potential of LiMnPO₄ is compatible with most of the currently used liquid electrolytes.^[14–19] However, the electrical conductivity of LiMnPO₄ is lower than the already insulating LiFePO₄ by five orders of magnitude,^[14–19] making it challenging to achieve high capacity at high rates for LiMnPO₄ using methods developed for LiFePO₄.^[14–19] Doping LiMnPO₄ with Fe has been pursued to enhance conductivity and stability of the material in its charged form.^[20–25] Recently, Martha et al. have obtained improved capacity and rate performance for carbon-coated LiMn_{0.8}Fe_{0.2}PO₄ nanoparticles synthesized by a high-temperature solid-state reaction.^[23]

Graphene is an ideal substrate for growing and anchoring insulating materials for energy storage applications because of its high conductivity, light weight, high mechanical strength, and structural flexibility.^[26–28] The electrochemical

performance of various electrode materials can be significantly boosted by rendering them conducting with graphene sheets.^[29–32] Recent work has shown improved specific capacities and rate capabilities of simple oxide nanomaterials (Mn₃O₄, Co₃O₄, and Fe₃O₄) grown on graphene as LIB anode materials.^[30–32] However, it remains a challenge to grow nanocrystals on graphene sheets in solution for materials with more sophisticated compositions and structures, such as LiMn_{1-x}Fe_xPO₄, which is a promising but extremely insulating cathode material for LIBs.

Herein we present a two-step approach for synthesis of LiMn_{1-x}Fe_xPO₄ nanorods on reduced graphene oxide sheets stably suspended in solution. Fe-doped Mn₃O₄ nanoparticles were first selectively grown onto graphene oxide by controlled hydrolysis. The oxide nanoparticle precursors then reacted solvothermally with Li and phosphate ions and were transformed into LiMn_{1-x}Fe_xPO₄ on the surface of reduced graphene oxide sheets. With a total content of 26 wt% conductive carbon, the resulting hybrid of nanorods and graphene showed high specific capacity and unprecedentedly high power rate for LiMn_{1-x}Fe_xPO₄ type of cathode materials. Stable capacities of 132 mAhg⁻¹ and 107 mAhg⁻¹ were obtained at high discharge rates of 20C and 50C, which is 85% and 70% of the capacity at C/2 (155 mAhg⁻¹), respectively. This affords LIBs with both high energy and high power densities. This is also the first synthesis of LiMn_{0.75}Fe_{0.25}PO₄ nanorods that have an ideal crystal shape and morphology for fast Li⁺ diffusion along the radial [010] direction of the nanorods.

Figure 1 shows our two-step solution-phase reaction for the synthesis LiMn_{0.75}Fe_{0.25}PO₄ nanorods on reduced graphene oxide (for experimental details, see the Supporting Information). The first step was to selectively grow oxide nanoparticles at 80 °C on mildly oxidized graphene oxide (mGO) stably suspended in a solution. Controlling the hydrolysis rate of Mn(OAc)₂ and Fe(NO₃)₃ by adjusting the H₂O/*N,N*-dimethylformamide (DMF) solvent ratio and the reaction temperature afforded selective and uniform coating of circa 10 nm nanoparticles of Fe-doped Mn₃O₄ (Supporting Information, Figure S1a; X-ray diffraction data in Figure S1b) on the mGO sheets without free growth of nanoparticles in solution. Importantly, our mGO was made by a modified Hummers method (Supporting Information), with which a sixfold lower concentration of KMnO₄ oxidizer was used to afford milder oxidation of graphite.^[33–36] The resulting mGO sheets contained a lower oxygen content than Hummers' GO (ca. 15% vs. ca. 30% measured by X-ray photoelectron spectroscopy (XPS) and Auger spectroscopy) and showed higher electrical conductivity when chemically reduced than

[*] H. Wang,^[†] Y. Liang, H. Sanchez Casalongue, Y. Li, G. Hong, Prof. H. Dai
Department of Chemistry
Stanford University, Stanford, CA 94305 (USA)
E-mail: hdai@stanford.edu
Y. Yang,^[†] L. Cui, Prof. Y. Cui
Department of Materials Science and Engineering
Stanford University, Stanford, CA 94305 (USA)
E-mail: yicui@stanford.edu

[†] These authors contributed equally to this work.

[**] This work is supported partially by the Office of Naval Research, NSF CHE-0639053, the LDRD Funding from the DOE SLAC Accelerator National Laboratory, and a Stanford Graduate Fellowship.

Supporting information for this article is available on the WWW under <http://dx.doi.org/10.1002/ange.201103163>.

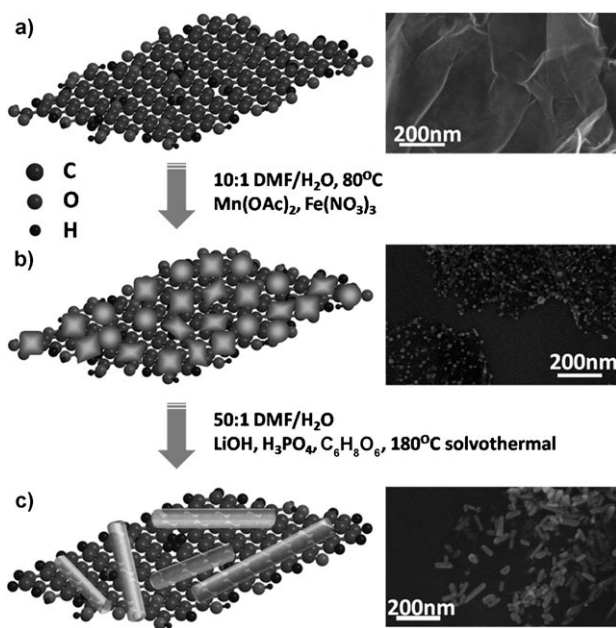


Figure 1. $\text{LiMn}_{0.75}\text{Fe}_{0.25}\text{PO}_4$ nanorod growth on rmGO. a) Ball-and-stick representation (left) and SEM image (right) of mGO. b) Representation of the structure (left) and SEM image (right) of Fe-doped Mn_3O_4 precursor nanoparticles grown on mGO after the first step of reaction at 80°C . c) Representation of the structure (left) and SEM image (right) of $\text{LiMn}_{0.75}\text{Fe}_{0.25}\text{PO}_4$ nanorods grown on rmGO after the second step of solvothermal reaction at 180°C .

Hummer's GO. Our mGO still contained sufficient functional groups, such as carboxyl, hydroxy, and epoxide groups for nucleating and anchoring oxide nanoparticles on the surface.^[30]

The second step transformed the Fe-doped Mn_3O_4 nanoparticles on mGO into $\text{LiMn}_{0.75}\text{Fe}_{0.25}\text{PO}_4$ nanorods (Figure 1), by reacting with LiOH and H_3PO_4 solvothermally at 180°C . Ascorbic acid ($\text{C}_6\text{H}_8\text{O}_6$) was added to reduce Fe^{III} to Fe^{II} and also to reduce mGO.^[37,38] The reduction is highly effective owing to the solvothermal conditions (oxygen content was reduced to about 4% as revealed by XPS; Supporting Information, Figure S2).^[36] This method afforded highly conducting reduced mildly oxidized graphene oxide sheets (rmGO) with the formation of $\text{LiMn}_{0.75}\text{Fe}_{0.25}\text{PO}_4$ nanorods atop. The electrical conductivity measured from pellets of $\text{LiMn}_{0.75}\text{Fe}_{0.25}\text{PO}_4/\text{rmGO}$ hybrid was measured to be $0.1\text{--}1\text{ Scm}^{-1}$, which is $10^{13}\text{--}10^{14}$ times higher than pure LiMnPO_4 .

Scanning electron microscopy (SEM) and transmission electron microscopy (TEM) revealed selective growth of single-crystalline $\text{LiMn}_{0.75}\text{Fe}_{0.25}\text{PO}_4$ nanorods on rmGO (Figure 2a,c), with a rod length of $50\text{--}100\text{ nm}$ and diameter of $20\text{--}30\text{ nm}$. High-resolution TEM showed the crystal lattice fringes throughout the entire $\text{LiMn}_{0.75}\text{Fe}_{0.25}\text{PO}_4$ nanorod formed on rmGO (Figure 2d), indicating the $\text{LiMn}_{0.75}\text{Fe}_{0.25}\text{PO}_4$ nanorods were single crystals. The X-ray diffraction peaks of the nanorods were slightly shifted to larger 2θ angles compared to pure LiMnPO_4 owing to Fe doping (Figure 2b)^[20–25] homogeneously in a solid solution (Figure 2d). Energy-dispersive spectroscopy (EDS) showed that the Mn/Fe ratio was about three in the nanorods

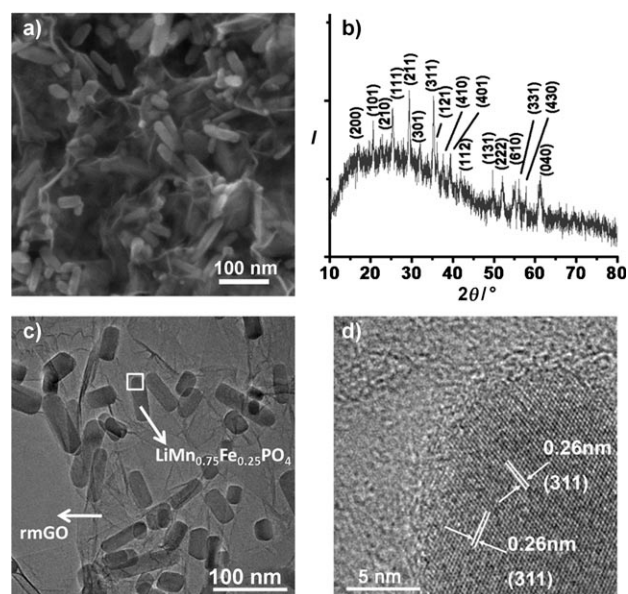
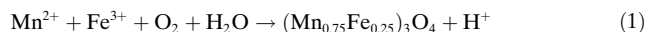


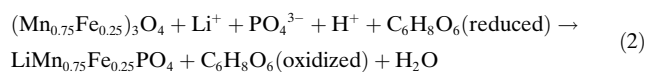
Figure 2. $\text{LiMn}_{0.75}\text{Fe}_{0.25}\text{PO}_4$ nanorods grown on rmGO. a) SEM image of the $\text{LiMn}_{0.75}\text{Fe}_{0.25}\text{PO}_4/\text{rmGO}$ hybrid. b) XRD spectrum of a packed thick film of $\text{LiMn}_{0.75}\text{Fe}_{0.25}\text{PO}_4/\text{rmGO}$. c) TEM image of $\text{LiMn}_{0.75}\text{Fe}_{0.25}\text{PO}_4/\text{rmGO}$. d) High-resolution TEM image of an individual $\text{LiMn}_{0.75}\text{Fe}_{0.25}\text{PO}_4$ nanorod on rmGO (boxed area in (c)).

(Supporting Information, Figure S3). The amount of rmGO in the hybrid was found to be about 20% by mass using thermal analysis (Supporting Information).

After the first step, we observed uniform coating of Mn/Fe oxide on mGO, a result of metal cation adsorption on the functional groups on mGO and hydrolysis [Eq. (1)]:



which afforded small oxide nanoparticles on mGO. The reaction was carried out in an open system exposed to air. The second step, the solvothermal reaction between the Mn/Fe oxide nanoparticles with Li and phosphate ions, afforded $\text{LiMn}_{0.75}\text{Fe}_{0.25}\text{PO}_4$ specifically on the surface of mGO accompanied by mGO reduction [Eq. (2)]:



By systematically varying the reaction time, we observed a gradual transformation of precursor particles into phosphate nanorods on rmGO (Supporting Information, Figures S4,S5).

In a control experiment, the same synthetic steps without mGO added produced irregularly shaped $\text{LiMn}_{0.75}\text{Fe}_{0.25}\text{PO}_4$ particles without the desired nanorod morphology (Supporting Information, Figure S6). Thus, our results suggested that mildly oxidized graphene sheets presented a unique substrate for growing nanocrystals into well-defined morphologies, such as nanoplates^[27] and nanorods. While the functional groups on mGO allow adsorption of cations and nanoparticle nucleation to achieve uniform precursor coating in the first step of reaction, the conjugated graphitic regions of rmGO (formed by reduction of mGO under solvothermal condi-

tions) interact with surface species weakly to promote the formation of well-defined shapes of nanocrystals in the second step of the reaction. The resulting nanorods could be bonded to rmGO by Mn/Fe–O–C bonds at the remaining oxygen sites and by van der Waals interactions with the aromatic regions of rmGO.

The nanoscale sizes (length 50–100 nm, width 20–30 nm) of the $\text{LiMn}_{0.75}\text{Fe}_{0.25}\text{PO}_4$ nanorods were desirable owing to decreased transport length for Li ions and electrons.^[8,13,15] High-resolution TEM analysis revealed that the long axes of the nanorods grown on rmGO were along the [001] axis of the $\text{LiMn}_{0.75}\text{Fe}_{0.25}\text{PO}_4$ crystal structure (Figure 3c,d, interplanar distance of (001) was ca. 0.47 nm). More importantly, the [010] axis, which is the Li^+ diffusion channel direction in

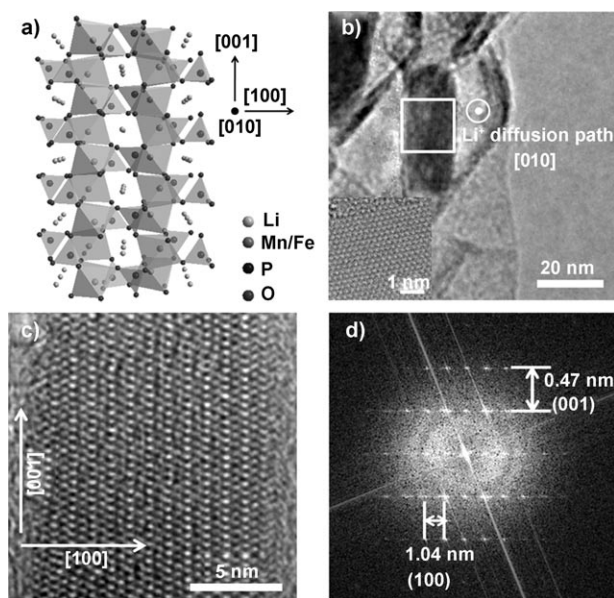


Figure 3. High-resolution TEM analysis of an individual $\text{LiMn}_{0.75}\text{Fe}_{0.25}\text{PO}_4$ nanorod grown on rmGO. a) Representation of the crystal structure of $\text{LiMn}_{0.75}\text{Fe}_{0.25}\text{PO}_4$. The lithium diffusion channels are clearly shown to be along the [010] direction (perpendicular to the figure plane). b) TEM image of a $\text{LiMn}_{0.75}\text{Fe}_{0.25}\text{PO}_4$ nanorod grown on rmGO. Inset: aberration-corrected TEM lattice image of an rmGO sheet. c) High-resolution TEM image of the $\text{LiMn}_{0.75}\text{Fe}_{0.25}\text{PO}_4$ nanorod on rmGO (boxed area in (b)). d) Fast Fourier transform of the lattice structure in (c). The growth direction of the $\text{LiMn}_{0.75}\text{Fe}_{0.25}\text{PO}_4$ nanorod is [001], and the lithium diffusion channel [010] is one of the short axes of the nanorods (perpendicular to the figure plane).

olivine type of crystals (Figure 3a),^[8,13,14,17] was along one of the short axes of the nanorods (Figure 3c,d, interplanar distance of (100) was ca. 1.04 nm). This short diffusion length could be ideal for fast Li^+ insertion and extraction with the $\text{LiMn}_{0.75}\text{Fe}_{0.25}\text{PO}_4$ nanorods/rmGO hybrid as the cathode of a lithium ion battery. Small diameters of the $\text{LiMn}_{0.75}\text{Fe}_{0.25}\text{PO}_4$ nanorods result in large surface areas and thus facilitate fast Li ion transport at the interface between the $\text{LiMn}_{0.75}\text{Fe}_{0.25}\text{PO}_4$ nanorods and the electrolyte. The Li^+ channels along the radial direction of the nanorods also favor rapid Li ion diffusion within the nanorods.

Coin cells were made to test the electrochemical performance of our $\text{LiMn}_{0.75}\text{Fe}_{0.25}\text{PO}_4$ nanorods/rmGO hybrid material (after annealing at 600 °C for 1 h) as the cathode (at a loading of ca. 3 mg cm⁻²) and with a Li foil as the anode. Figure 4a showed the typical charge and discharge curves of our material at a rate of C/2 (all C rates based on the

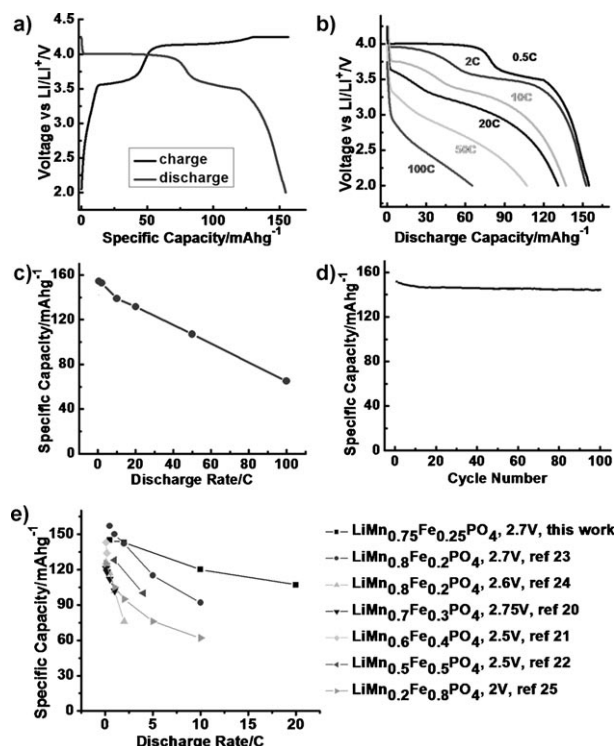


Figure 4. Electrochemical characterizations of the $\text{LiMn}_{0.75}\text{Fe}_{0.25}\text{PO}_4$ nanorod cathode grown on rmGO. a) Representative charge and discharge curves of $\text{LiMn}_{0.75}\text{Fe}_{0.25}\text{PO}_4$ nanorods grown on rmGO at a rate of C/2. b) Discharge curves of $\text{LiMn}_{0.75}\text{Fe}_{0.25}\text{PO}_4$ nanorods on rmGO at various C rates. c) Specific discharge capacities of $\text{LiMn}_{0.75}\text{Fe}_{0.25}\text{PO}_4$ nanorods on rmGO at various C rates. The discharge cut-off voltage was 2.0 V vs Li^+/Li . d) Capacity retention of $\text{LiMn}_{0.75}\text{Fe}_{0.25}\text{PO}_4$ nanorods on rmGO at the rate of C/2. e) Comparison of rate capability of $\text{LiMn}_{0.75}\text{Fe}_{0.25}\text{PO}_4$ nanorods grown on rmGO with other Fe-doped LiMnPO_4 cathode materials. The discharge cut-off voltages are listed in the legend on the right.

theoretical specific capacity of $\text{LiMn}_{0.75}\text{Fe}_{0.25}\text{PO}_4$, where a 1C rate corresponds to a current density of 170 mA g⁻¹). The charge curve has two voltage plateaus at about 3.6 V and about 4.2 V, corresponding to the oxidation from Fe^{II} to Fe^{III} and from Mn^{II} to Mn^{III} , respectively.^[20–25] The capacity of the 3.6 V plateau was about one-third of that of the 4.2 V plateau, consistent with the Fe/Mn ratio of the $\text{LiMn}_{0.75}\text{Fe}_{0.25}\text{PO}_4$ nanorods. The discharge curve also showed two voltage plateaus at about 4.0 V and about 3.5 V owing to reduction from Mn^{III} to Mn^{II} and from Fe^{III} to Fe^{II} , respectively.

Figure 4b showed the discharge curves at various rates for our $\text{LiMn}_{0.75}\text{Fe}_{0.25}\text{PO}_4$ nanorods/rmGO cathode material (see the Supporting Information, Figure S7 for another data set from a different batch of $\text{LiMn}_{0.75}\text{Fe}_{0.25}\text{PO}_4$ nanorods/rmGO hybrid material). Charging was done at a C/2 constant current

to 4.25 V followed by a constant voltage charging at 4.25 V with a cut-off current of $C/20$. At a $C/2$ discharge rate and 2.0 V cut-off voltage, our material showed a specific capacity of 155 mAh g^{-1} based on the mass of the active material $\text{LiMn}_{0.75}\text{Fe}_{0.25}\text{PO}_4$ (Figure 4c), which is 91 % of the theoretical capacity. The capacity remained high at 153 mAh g^{-1} at a discharge rate of 2C. At a high discharge rate of 20C, the capacity was still as high as 132 mAh g^{-1} . For even higher discharge rates, we obtained a capacity of 107 mAh g^{-1} at 50C, and 65 mAh g^{-1} at 100C (corresponding to a discharge time of 36 s for theoretical capacity). A cut-off voltage of 2.0 V was used for all the discharge rates above (Figure 4b).

Our nanorod/graphene hybrid material exhibited the highest rate performance measured by similar voltage cut-off conditions among all pure and doped LiMnPO_4 cathode materials (see Figure 4e for comparison, we used a 2.7 V cut-off voltage in this case). Notably, the rate performance of our $\text{LiMn}_{0.75}\text{Fe}_{0.25}\text{PO}_4$ nanorods/rmGO hybrid was also comparable to some of the best reported cathode materials (including LiFePO_4 , LiCoO_2 , and LiMn_2O_4) with ultrahigh rate capabilities (Supporting Information, Figure S8).^[10,12,39–41] Moreover, the content of conductive carbon in our work was only 26 % including both rmGO and carbon black, which was much lower than that used previously for discharging rates $\geq 100 \text{ C}$ (45 % carbon or higher).^[10,39,41] Further, our material exhibited good cycle life, showing little capacity decay (ca. 1.9 %) for 90 cycles from the 11th to the 100th cycle (Figure 4d). The Coulombic efficiency (CE) was typically higher than 99.0 %. After 50 cycles, the CE was higher than 99.5 %, suggesting little side chemical reaction or stable solid electrolyte interphase (SEI) formation between electrolyte and $\text{LiMn}_{0.75}\text{Fe}_{0.25}\text{PO}_4$ nanorods/rmGO hybrid.^[14]

The outstanding electrochemical performance of our $\text{LiMn}_{0.75}\text{Fe}_{0.25}\text{PO}_4$ /rmGO hybrid material for lithium ion batteries was attributed to the intimate interactions between the nanorods and the underlying reduced graphene oxide sheets, and the small size and ideal nanorod morphology and crystallographic orientation of the $\text{LiMn}_{0.75}\text{Fe}_{0.25}\text{PO}_4$ nanocrystals. In a control experiment, a physical mixture of $\text{LiMn}_{0.75}\text{Fe}_{0.25}\text{PO}_4$ nanoparticles and rmGO sheets showed much lower specific capacities even at low rates (75 mAh g^{-1} at $C/10$ and 44 mAh g^{-1} at 1C rate; Supporting Information, Figure S9a, S9b). The capacity of the mixture further decreased to less than 2 mAh g^{-1} at a discharge rate of 50 C, clearly showing that the capacity contribution of rmGO at high rate is negligible (Supporting Information, Figure S9c). Electrochemical impedance spectroscopy (EIS) provided strong evidence of significantly improved charge transport in the cathode made of $\text{LiMn}_{0.75}\text{Fe}_{0.25}\text{PO}_4$ nanorods directly grown on rmGO over the simple physical mixture (Supporting Information, Figure S10). Cyclic voltammetry (CV) measurements also showed much better charge and discharge kinetics of $\text{LiMn}_{0.75}\text{Fe}_{0.25}\text{PO}_4$ nanorods directly grown on rmGO compared to the physical mixture of $\text{LiMn}_{0.75}\text{Fe}_{0.25}\text{PO}_4$ and rmGO (Supporting Information, Figure S11).

In summary, we have developed the first synthesis of complex single-crystalline nanomaterials on highly conducting mildly oxidized graphene sheets with desired size and morphology. The resulting high electrical conductivity and

low ionic resistance led to excellent rate performance for the otherwise extremely insulating $\text{LiMn}_{0.75}\text{Fe}_{0.25}\text{PO}_4$ cathode material. This work opens the door to complex hybrid materials design and engineering with graphene for advanced energy storage.

Received: May 9, 2011

Published online: June 27, 2011

Keywords: graphene · high-rate cathodes · lithium ion batteries · nanomaterials

- [1] M. S. Whittingham, *Chem. Rev.* **2004**, *104*, 4271–4301.
- [2] B. L. Ellis, K. T. Lee, L. F. Nazar, *Chem. Mater.* **2010**, *22*, 691–714.
- [3] P. G. Bruce, B. Scrosati, J. Tarascon, *Angew. Chem.* **2008**, *120*, 2972–2989; *Angew. Chem. Int. Ed.* **2008**, *47*, 2930–2946.
- [4] A. V. Murugan, T. Muraliganth, P. J. Ferreira, A. Manthiram, *Inorg. Chem.* **2009**, *48*, 946–952.
- [5] A. K. Padhi, K. S. Nanjundaswamy, J. B. Goodenough, *J. Electrochem. Soc.* **1997**, *144*, 1188–1194.
- [6] A. Yamada, S. C. Chung, K. Hinokuma, *J. Electrochem. Soc.* **2001**, *148*, A224–A229.
- [7] H. Huang, S. Yin, L. F. Nazar, *Electrochem. Solid-State Lett.* **2001**, *4*, A170–A172.
- [8] C. Delacourt, P. Poizot, S. Levasseur, C. Masquelier, *Electrochem. Solid-State Lett.* **2006**, *9*, A352–A355.
- [9] Y. Wang, Y. Wang, E. Hosono, K. Wang, H. Zhou, *Angew. Chem.* **2008**, *120*, 7571–7575; *Angew. Chem. Int. Ed.* **2008**, *47*, 7461–7465.
- [10] B. Kang, G. Cedar, *Nature* **2009**, *458*, 190–193.
- [11] S. W. Oh, S. Myung, S. Oh, K. H. Oh, K. Amine, B. Scrosati, Y. Sun, *Adv. Mater.* **2010**, *22*, 4842–4845.
- [12] W. Zhang, *J. Electrochem. Soc.* **2010**, *157*, A1040–A1046.
- [13] D. Kim, J. Kim, *Electrochem. Solid-State Lett.* **2006**, *9*, A439–A442.
- [14] L. Wang, F. Zhou, G. Ceder, *Electrochem. Solid-State Lett.* **2008**, *11*, A94–A96.
- [15] T. Drezen, N. Kwon, P. Bowen, I. Teerlinck, M. Isono, I. Exnar, *J. Power Sources* **2007**, *174*, 949–953.
- [16] S. K. Martha, B. Markovsky, J. Grinblat, Y. Gofer, O. Haik, E. Zinigrad, D. Aurbach, T. Drezen, D. Wang, G. Deghenghi, I. Exnar, *J. Electrochem. Soc.* **2009**, *156*, A541–A552.
- [17] D. Choi, D. Wang, I. Bae, J. Xiao, Z. Nie, W. Wang, V. V. Viswanathan, Y. J. Lee, J. Zhang, G. L. Graff, Z. Yang, J. Liu, *Nano Lett.* **2010**, *10*, 2799–2805.
- [18] Z. Bakenov, I. Taniguchi, *J. Power Sources* **2010**, *195*, 7445–7451.
- [19] B. Kang, G. Cedar, *J. Electrochem. Soc.* **2010**, *157*, A808–A811.
- [20] X. Chang, Z. Wang, X. Li, L. Zhang, H. Guo, W. Peng, *Mater. Res. Bull.* **2005**, *40*, 1513–1520.
- [21] C. H. Mi, X. G. Zhang, X. B. Zhao, H. L. Li, *Mater. Sci. Eng. B* **2006**, *129*, 8–13.
- [22] K. Zaghib, A. Mauger, F. Gendron, M. Massot, C. M. Julien, *Ionics* **2008**, *14*, 371–376.
- [23] S. K. Martha, J. Grinblat, O. Haik, E. Zinigrad, T. Drezen, J. H. Miners, I. Exnar, A. Kay, B. Markovsky, D. Aurbach, *Angew. Chem.* **2009**, *121*, 8711–8715; *Angew. Chem. Int. Ed.* **2009**, *48*, 8559–8563.
- [24] B. Zhang, X. Wang, Z. Liu, H. Li, X. Huang, *J. Electrochem. Soc.* **2010**, *157*, A285–A288.
- [25] Y. Wang, D. Zhang, X. Yu, R. Cai, Z. Shao, X. Liao, Z. Ma, *J. Alloys Compd.* **2010**, *492*, 675–680.
- [26] S. Park, R. S. Ruoff, *Nat. Nanotechnol.* **2009**, *4*, 217–224.

- [27] H. Wang, J. T. Robinson, G. Diankov, H. Dai, *J. Am. Chem. Soc.* **2010**, *132*, 3270–3271.
- [28] Y. Liang, H. Wang, H. S. Casalongue, Z. Chen, H. Dai, *Nano Res.* **2010**, *3*, 701–705.
- [29] H. Wang, H. Sanchez Casalongue, Y. Liang, H. Dai, *J. Am. Chem. Soc.* **2010**, *132*, 7472–7477.
- [30] H. Wang, L. Cui, Y. Yang, H. S. Casalongue, J. T. Robinson, Y. Liang, Y. Cui, H. Dai, *J. Am. Chem. Soc.* **2010**, *132*, 13978–13980.
- [31] S. Yang, G. Cui, S. Pang, Q. Cao, U. Kolb, X. Feng, J. Maier, K. Mullen, *ChemSusChem* **2010**, *3*, 236–239.
- [32] M. Zhang, D. Lei, X. Yin, L. Chen, Q. Li, Y. Wang, T. Wang, *J. Mater. Chem.* **2010**, *20*, 5538–5543.
- [33] W. S. Hummers, R. E. Offeman, *J. Am. Chem. Soc.* **1958**, *80*, 1339–1339.
- [34] H. Wang, X. Wang, X. Li, H. Dai, *Nano Res.* **2009**, *2*, 336–342.
- [35] X. Sun, Z. Liu, K. Welsher, J. T. Robinson, A. Goodwin, S. Zaric, H. Dai, *Nano Res.* **2008**, *1*, 203–212.
- [36] H. Wang, J. Robinson, X. Li, H. Dai, *J. Am. Chem. Soc.* **2009**, *131*, 9910–9911.
- [37] M. J. Fernández-Merino, L. Guardia, J. I. Paredes, S. Villar-Rodil, P. Solís-Fernández, A. Martínez-Alonso, J. M. D. Tascón, *J. Phys. Chem. C* **2010**, *114*, 6426–6432.
- [38] J. Gao, F. Liu, Y. Liu, N. Ma, Z. Wang, X. Zhang, *Chem. Mater.* **2010**, *22*, 2213–2218.
- [39] M. Okubo, E. Hosono, J. Kim, M. Enomoto, N. Kojima, T. Kudo, H. Zhou, I. Honma, *J. Am. Chem. Soc.* **2007**, *129*, 7444–7452.
- [40] K. M. Shaju, P. G. Bruce, *Chem. Mater.* **2008**, *20*, 5557–5562.
- [41] E. Hosono, T. Kudo, I. Honma, H. Matsuda, H. Zhou, *Nano Lett.* **2009**, *9*, 1045–1051.